
POINT CLOUD REGISTRATION USING REPRESENTATIVE OVERLAPPING POINTS

Lifa Zhu
DeepGlint
Beijing, China
lifazhu@deepglint.com

Dongrui Liu
Shanghai Jiao Tong University
Shanghai, China
drliu96@sjtu.edu.cn

Changwei Lin
DeepGlint
Beijing, China
changweilin@deepglint.com

Rui Yan
Institute of Computing Technology, Chinese Academy of Sciences
Beijing, China
yanrui20b@ict.ac.cn

Francisco Gómez-Fernández
DeepGlint
Beijing, China
francisco@deepglint.com

Ninghua Yang
DeepGlint
Beijing, China
ninghuayang@deepglint.com

Ziyong Feng
DeepGlint
Beijing, China
ziyongfeng@deepglint.com

ABSTRACT

3D point cloud registration is a fundamental task in robotics and computer vision. Recently, many learning-based point cloud registration methods based on correspondences have emerged. However, these methods heavily rely on such correspondences and meet great challenges with partial overlap. In this paper, we propose ROPNet, a new deep learning model using Representative Overlapping Points with discriminative features for registration that transforms partial-to-partial registration into partial-to-complete registration. Specifically, we propose a context-guided module which uses an encoder to extract global features for predicting point overlap score. To better find representative overlapping points, we use the extracted global features for coarse alignment. Then, we introduce a Transformer to enrich point features and remove non-representative points based on point overlap score and feature matching. A similarity matrix is built in a partial-to-complete mode, and finally, weighted SVD is adopted to estimate a transformation matrix. Extensive experiments over ModelNet40 using noisy and partially overlapping point clouds show that the proposed method outperforms traditional and learning-based methods, achieving state-of-the-art performance. The source code is publicly available at <https://github.com/zhu1f0804/ROPNet>.

1 Introduction

Rigid point cloud registration is a fundamental task in computer vision and robotics, aiming to find the rigid transformation that aligns a pair of point clouds. It has many important applications in scene reconstruction [1, 2, 3], positioning and localization [4, 5], object pose estimation [6] and so on. Partially overlapping point cloud registration, i.e., partial-to-partial registration, is a common task in the real world. Robotic platforms equipped with modern depth cameras most of the time produce partially overlapping 3D point clouds due to the small camera motion between consecutive frames. In addition, in 3D reconstruction tasks, in order to produce a complete 3D scene, overlapping point clouds are captured from different shooting angles.

Traditional methods, such as ICP [7], Go-ICP [8], and FGR [9], are widely used for rigid point cloud registration. However, they are sensitive to noise and partially overlapping point clouds. Recently, learning-based methods [10, 11, 12, 13, 14, 15, 16, 17, 18] have shown to be more robust, especially for partial-to-partial registration. PRNet [13], IDAM [14] and RPMNet [15] solve partial-to-partial registration in different ways: by generating a sharp matching

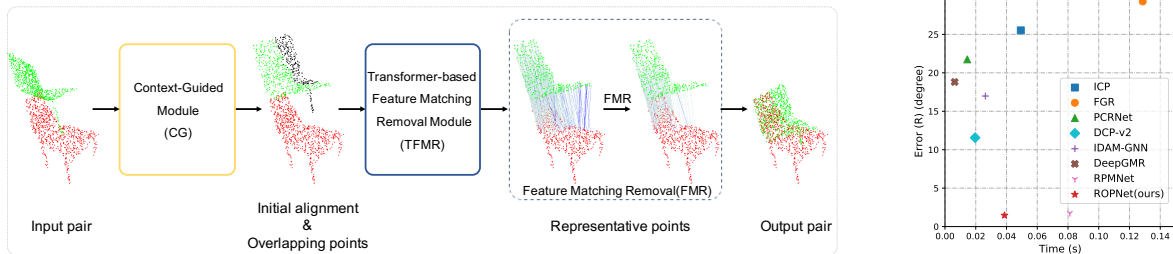


Figure 1: Left: Overview of ROPNet registration pipeline. The CG module consumes the source (green) and target (red) point clouds, and outputs initial pose and overlapping points (non-overlapping points are in black). The TFMR module takes the output of CG module as input, and generates accurate correspondences. The FMR step removes false correspondences (blue lines) and keeps some positive correspondences (gray lines). Right: Error(R)-time comparison of different methods. Our ROPNet achieves the lowest $Error(R)$ with a moderate speed.

function based on keypoints with Gumbel-Softmax [19]; using a hybrid point elimination with a mutual-supervised loss, and applying iterative Sinkhorn [20] layers to generate a doubly stochastic matrix. However, none of them explicitly deal with *non-overlapping points*, i.e. points without a matching pair between source and target point clouds, which are critical for registration. To the best of our knowledge, PREDATOR [16] is the first work to explicitly deal with non-overlapping points. Despite its good performance, when some overlapping points are mistakenly removed from the target point cloud, false correspondences may be produced affecting the registration.

Up to now, partial-to-partial registration is still not well resolved. Finding a few accurate correspondences is sufficient to solve the partial-to-partial registration problem. Although descriptive point features are essential to establish good point correspondences, they are always sensitive to rotation transformations. Even using rotation-invariant features, there may still be some false point correspondences due to the existence of noisy or non-overlapping points. Removing non-overlapping points in the source point cloud can effectively guarantee that each point in the source point cloud has a corresponding point in the target point cloud. We call this *partial-to-complete* registration where *complete* means the target point cloud is complete compared to the source point cloud.

Based on the above discussions, we propose *ROPNet* for rigid partial-to-partial point cloud registration using representative overlapping points. First, we present a simple yet effective context-guided (CG) module to predict a point overlap score. The point overlap score is obtained through the information interaction between the point features and the global features from the pair. To better find representative overlapping points, we regress a rough initial transformation based on the global features. Second, we propose a Transformer-based feature matching removal (TFMR) module, which employs a point cloud Transformer for enriching point features and estimate a similarity matrix based on features to obtain representative overlapping points. Then, we remove non-representative points from the source point cloud and transform partial-to-partial registration to partial-to-complete registration. Finally, weighted SVD is employed to estimate the transformation matrix. Combining transformations from CG and TFMR modules, an accurate transformation matrix $T \in SE(3)$ are finally calculated. The pipeline of our proposed ROPNet is shown in Figure 1.

Extensive experiments showed that the proposed method achieves state-of-the-art performance on noisy and partially overlapping point clouds, outperforming traditional and learning-based methods.

2 Related Work

2.1 Traditional registration

The ICP algorithm [7] iteratively alternates between two main steps until a desired stopping criteria is met: i) point correspondences computation between source and target point clouds, ii) rigid body transformation estimation by solving the least square problem. The variant point-to-plane ICP [21, 22] uses a different objective function, which requires normal vectors for the target point cloud, that has been shown a better and faster convergence. However, ICP and its variants are sensitive to initial alignment and noisy points, and also they easily fall into a local optimal.

Another family of registration algorithms, known as global registration, computes a rough transformation to align source and target point clouds [23, 8, 9]. The branch-and-bound methods, e.g. Go-ICP [8], systematically search for the optimal solution in the pose space. RANSAC-based [23] methods randomly pick in each iteration a fixed number

of points from the source and target point clouds to estimate an alignment, and finally output the best transformation. However, the above methods are time-consuming, which is not acceptable in practical applications. FGR [9] extracts Fast Point Feature Histogram (FPFH) [24] descriptors to find good matching point pairs in a 33-dimensional feature space. However, handcrafted features are sensitive to noise and FGR doesn't work well on partial-to-partial registration.

2.2 Learning-based registration

Global features based methods, such as PointNetLK [10] and PCRNet [11], both use PointNet [25] to extract global features. PointNetLK uses a modified Lucas & Kanade (LK) algorithm [26] for aligning features to achieve registration. PCRNet replaces the LK algorithm with Multi-Layer Perceptron (MLP) to promote the robustness to the noisy points. They both capture global features for complete-to-complete registration, causing massive information loss and inaccurate transformations.

Correspondence-based Deep Closest Point (DCP) [12] learns point features, computes a distance matrix based on features, and generates virtual correspondences to solve the least square problem. DeepGMR [17] solves the point correspondence step by matching points using a Gaussian Mixture Model whose parameters are estimated by a neural network. PRNet [13] performs partial-to-partial registration by detecting keypoints and establishing keypoint-to-keypoint correspondences with Gumbel-Softmax [19]. RPMNet [15] solves partial-to-partial registration by applying iterative Sinkhorn [20] layers to generate a doubly stochastic matrix [20]. IDAM [14] incorporates both features and Euclidean information for correspondence matrix and uses a two-stage point elimination for partial-to-partial registration. The above correspondence-based methods solve the partial-to-partial registration problem indirectly or do not consider it at all.

RANSAC-based FCGF [27] uses a UNet [28] architecture with skip connections and residual blocks to extract fully-convolutional features. D3Feat [29] applies KPConv [30] as backbone to predict features and point saliency. PREDATOR [16] proposes an overlap-attention block for point feature extraction, overlap score and saliency prediction. However, the above RANSAC-based methods tend to be slow. In addition, mistakenly removal of non-overlapping points from the target point cloud may produce false matches.

3 Methods

The partial-to-partial rigid point cloud registration problem can be stated as follows. Given two input point clouds $X \in \mathbb{R}^{N \times 3}$ and $Y \in \mathbb{R}^{M \times 3}$, our goal is to find a rigid body transformation R, t that better aligns X to Y in the least-squares sense using a learned subset of overlapping point correspondences.

3.1 Context-guided module for initialization and overlap

We have observed that a rough initial registration is always favourable to point feature learning due to small rotation transformation. In SpinNet [31], it is shown that rotation-invariant features are hard to learn. Also, overlapping points can greatly improve the correspondence accuracy that are critical for registration [16]. Therefore, we propose a context-guided (CG) module for initialization and point overlapping score prediction. Figure 2 shows the CG architecture.

Initialization For simplicity, we use a modified PointNet network as the encoder of our CG module. Inspired by PCRNet [11], we use the encoder module to extract global features and regress a 7-dimensional vector representing a rotation and translation transformation. Then, the initial alignment can be formulated as:

$$v = h_\phi(\text{cat}(\max(f_\theta(X)), \max(f_\theta(Y))))), \quad (1)$$

where $f_\theta(\cdot)$ denotes the shared encoder module which learns a high-dimensional feature $F_X \in \mathbb{R}^{N \times C}$ and $F_Y \in \mathbb{R}^{M \times C}$ for the source X and target Y input point clouds. The symbol $\max(\cdot)$ denotes max-pooling and cat represents concatenation. The transformation decoder is denoted as $h_\phi(\cdot)$ which is a simple Multiple-Layer Perceptron (MLP). The first fourth values of v represent the quaternion rotation vector $q_0 \in \mathbb{R}^4$ that are used to calculate the initial transformation matrix R_0 , and the last three values represent the translation $t_0 \in \mathbb{R}^3$. The transformed source point cloud X' can be obtained by $X' = X \cdot R_0^T + t_0^T$, abusing notation for the summation of t_0 which is done row by row.

Overlap Information from both source and target point cloud is essential for overlapping points prediction. Thus, we design a simple information interaction module for overlapping points prediction based on global features. These features are obtained from the initialization step, saving computation. Here, we formulate the overlap prediction

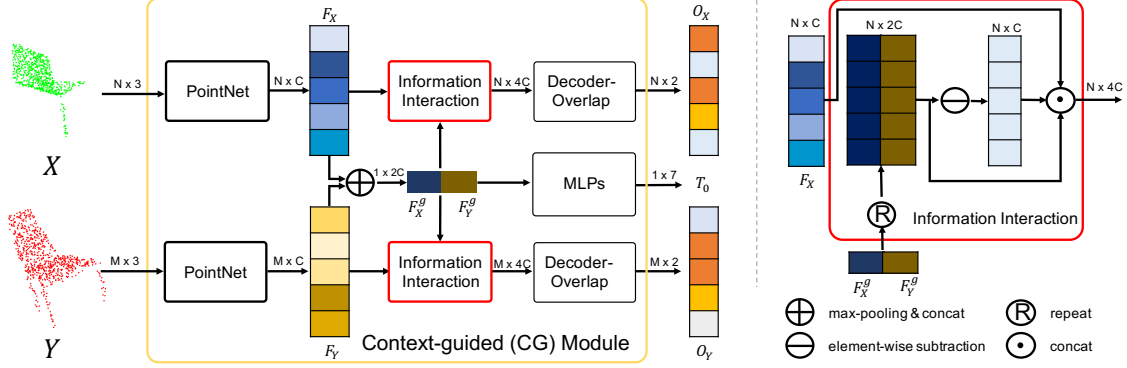


Figure 2: Left: Architecture of the CG module. CG module consumes source X (in green) and target Y (in red) data, and outputs overlap score (O_X, O_Y) and initial transformation matrix T_0 . Right: Details of information interaction. It takes point features and global features as input and outputs fused point features based on the pair.

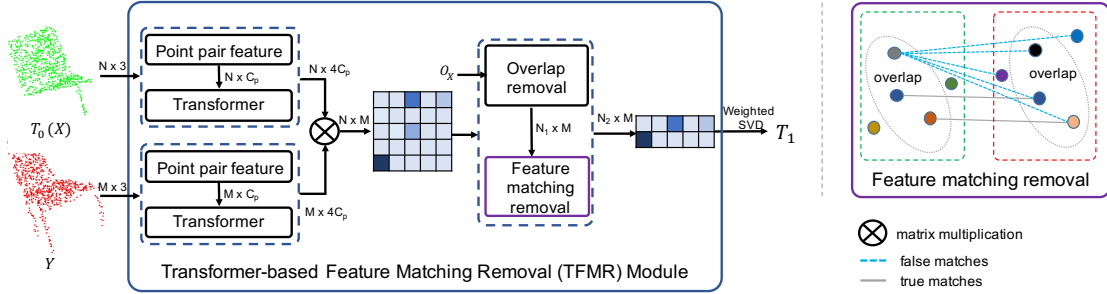


Figure 3: Left: Overview of Transformer-based feature matching removal (TFMR) module. TFMR module takes the transformed source X' and target Y as input, and outputs representative points and their correspondences. T_0 and O_X are the output from CG module that denote initial alignment and overlap score for X . Right: Details of feature matching removal (FMR). It takes correspondences for overlapping source points and outputs accurate correspondences (gray lines).

problem as a binary classification task. The overlap score can be calculated as:

$$\begin{aligned} O_X &= g_\psi(\text{cat}(F_X, r(F_X^g), r(F_Y^g), r(F_X^g - F_Y^g))), \\ O_Y &= g_\psi(\text{cat}(F_Y, r(F_Y^g), r(F_X^g), r(F_Y^g - F_X^g))), \end{aligned} \quad (2)$$

where $r(\cdot)$ denotes expanding dimensions and repeating features, g_ψ is the overlap decoder (which is denoted in a PointNet-style) followed by a softmax function, and O_X and O_Y denote point overlap score of the source X and target Y point clouds. The parameters from g_ψ are shared among input point clouds.

3.2 Transformer-based feature matching removal

We refine the registration based on the point correspondences from transformed source X' and target Y . The proposed Transformer-based feature matching removal (TFMR) module removes non-representative points from X' . The architecture of the TFMR module is depicted in Figure 3.

Point pair feature Before Transformer, we implement point feature augmentation following RPMNet [15]. For each point $x \in \mathbb{X}'$, we obtain the k -nearest neighbor points $M_k \in \mathbb{R}^{k \times 3}$ within a predefined radius. We denote the augmented feature as $F_{m_i}^a \in \mathbb{R}^{10}$ for $m_i \in M_k$ which concatenates spatial coordinates and Point Pair Feature [32] $PPF_i \in \mathbb{R}^4$. Then we get the feature $F_x^p \in \mathbb{R}^{C_p}$ for the point x as:

$$F_{m_i}^a = [m_i, m_i - x, PPF_i], \quad F_x^p = \max_{1 \leq i \leq k} (\mu_\theta(F_{m_i}^a)), \quad (3)$$

where μ_θ consists of several 1-d convolution layers and max denotes max-pooling.

Transformer Point features require to consider global information. Transformer [33, 34, 35] integrates point features based on all input points, showing advantages over local features [36, 37, 30, 38, 39, 40]. Given an augmented feature

$F_{X'}^p \in \mathbb{R}^{N \times C_p}$ (abbreviated as $F_{X'}$ for convenience) for the transformed source point cloud X' , we generate point features based on self-attention as follows:

$$\begin{aligned} Q_i &= F_{X'}^i \cdot W_i^Q, & K_i &= F_{X'}^i \cdot W_i^K, & V_i &= F_{X'}^i \cdot W_i^V, \\ s_i &= \text{norm}(\text{softmax}(Q_i \cdot K_i^T)), & F_{X'}^{i+1} &= s_i \cdot V_i, \end{aligned} \quad (4)$$

where \cdot denotes matrix multiplication, i is the index of self-attention and $F_{X'}^0 = F_{X'}$, $W_i^Q \in \mathbb{R}^{C_p \times C_0}$, $W_i^K \in \mathbb{R}^{C_p \times C_0}$ and $W_i^V \in \mathbb{R}^{C_p \times C_p}$ are learned weights and C_0 is a hyperparameter used to control the amount of calculation. The symbol $\text{softmax}(\cdot)$ denotes row softmax and $\text{norm}(\cdot)$ means column normalization. Following self-attention, the Feature Forward Neural Network (FFNN) is a residual network. Then, Transformer is composed of several self-attention and FFNN groups. The output features for X' and Y are represented as $F_{X'}^t \in \mathbb{R}^{N \times 4C_p}$ and $F_Y^t \in \mathbb{R}^{M \times 4C_p}$.

Feature matching removal We first compute the similarity matrix $H = F_{X'}^t \cdot F_Y^t{}^T$. However, there may exist points in X' without a corresponding point in Y , such that the correspondence matrix satisfies $\sum_j^M H_{ij} \leq 1, \forall i$. We can remove non-overlapping points in X' which guarantees the remaining points X'_{o1} to satisfy $\sum_j^M H_{o1,ij} = 1, \forall i$, so it is sufficient for solving partial-to-partial registration. In this way, we obtain representative overlapping points in two steps. First, we select top- N_1 points as overlapping points $X'_{o1} \in \mathbb{R}^{N_1 \times 3}$ based on the overlap score O_X predicted in the CG module. Second, we perform feature matching to further remove points whose features are not descriptive to obtain the final representative points:

$$X'_{o2} = X'_{o1} [\arg \max_{\text{top-prob}} (\max_j (F_{X'_{o1}}^t \cdot F_Y^t{}^T)_{ij})], \quad (5)$$

where top-prob means obtaining an amount of indices with top similarity scores in the probability proportion of prob . We then obtain the similarity matrix $H_{o2} = F_{X'_{o2}}^t \cdot F_Y^t{}^T$ for representative overlapping points which transforms partial-to-partial registration into partial-to-complete registration. For each point $x_{o2,i} \in X'_{o2}$, the corresponding point y_i is computed as following:

$$J = \arg \max_{\text{top-k}} H_{o2,i}, \quad w_{ij} = \begin{cases} H_{o2,ij} & j \in J \\ 0 & j \notin J \end{cases}, \quad y_i = \frac{w_{i,:}}{\sum_j w_{i,j}} \cdot Y, \quad (6)$$

where J denotes the indices of Y which have top- k maximum similarity scores for $x_{o2,i}$. To generate the set of correspondences, each point pair is defined as $(x_{o2,i}, y_i)$ with weight $O_{X'_{o2},i}$. Then, weighted SVD is used for estimating an accurate transformation $R_1 \in \mathbb{SO}(3)$ and $t_1 \in \mathbb{R}^3$. The final transformation is obtained by setting $R = R_1 \cdot R_0$, and $t = R_1 \cdot t_0 + t_1$.

3.3 Loss function

We adopt the widely used loss function which calculates the distance between predicted and ground truth transformed source data. Since we consider the prediction of the overlap score as a binary classification task, we supervise it with a cross-entropy loss. In addition, to make training more efficient, we adopt the same loss as R, t for initial R_0, t_0 as an auxiliary loss:

$$\begin{aligned} L_{fin} &= \|X \cdot R^T - X \cdot \hat{R}^T\|_1 + \|t - \hat{t}\|_1, & L_{init} &= \|X \cdot R_0^T - X \cdot \hat{R}^T\|_1 + \|t_0 - \hat{t}\|_1, \\ L_{ol} &= \frac{1}{2N} \sum_i \sum_j (\hat{O}_X)_{ij} \cdot \log(O_X)_{ij} + \frac{1}{2M} \sum_i \sum_j (\hat{O}_Y)_{ij} \cdot \log(O_Y)_{ij}, \end{aligned} \quad (7)$$

where \hat{R} and \hat{t} denotes the ground truth rotation matrix and translation vector, and \hat{O}_X and \hat{O}_Y represent the ground truth overlap score using the mapping Φ_X obtained by Equation 8,

$$\Phi_X = \{X_i | NN(\hat{R} \cdot X_i + \hat{t}, Y) < d, \forall i\}, \quad (8)$$

where $NN(x, Y)$ denotes finding the nearest neighbour in Y for the point x . Then, we set the score to 1 for correspondences below a predefined threshold d and 0 otherwise.

3.4 Implementation

ROPNet is implemented in PyTorch [41, 42] and all experiments were run on a Tesla V100 GPU with an Intel 6133 CPU at 2.50GHz CPU. For the CG module, the number of filters in the encoder are [64, 64, 64, 128, 512]. The number of filters in transformation and overlap decoder are [512, 512, 256, 7] and [512, 512, 256, 2], respectively. For the

Methods	AO				TO			
	$Error(R)$	$Error(t)$	$MAE(R)$	$MAE(t)$	$Error(R)$	$Error(t)$	$MAE(R)$	$MAE(t)$
ICP	23.4101	0.2493	11.6681	0.1147	24.6413	0.2525	12.1470	0.1171
FGR	14.3599	0.0927	8.4620	0.0440	14.0114	0.0978	8.2744	0.0462
PCRNet	24.7053	0.1997	11.3387	0.0966	24.3003	0.2000	11.2207	0.0969
DCP-v2	10.3151	0.1319	5.2299	0.0640	11.1723	0.1356	5.6421	0.0657
IDAM-GNN	13.6264	0.1886	7.1060	0.0862	14.2891	0.1909	7.4966	0.0877
DeepGMR	13.3886	0.1542	6.6794	0.0751	14.3612	0.1589	7.0914	0.0775
RPMNet	0.9335	0.0113	0.4860	0.0054	1.4239	0.0139	0.7304	0.0065
ROPNet	0.7820	0.0086	0.4146	0.0040	1.1567	0.0108	0.5946	0.0051

Table 1: Results on ModelNet40 unseen shapes.

TFMR module, we have four self-attention and FFNN layers where each output has 192 dimensions. We adopt Group Normalization (GN) [43] in the TFMR module. For the ModelNet40 dataset, we train for 600 epochs using Adam [44] with initial learning rate of 0.0001. The learning rate changes using a cosine annealing schedule [45]. We train ROPNet in a non-iterative manner. However, we run 2 iterations for the TFMR module during test.

4 Experiments

4.1 Dataset

ModelNet40 [46] is widely used for point cloud registration as conducted in recent learning-based methods [12, 11, 13, 15, 47, 48]. There are 12,311 CAD models from 40 categories, splitting into 9,843 for training and 2,468 for testing.

It is noted that there are some symmetrical objects in ModelNet40, including bottle, bowl, cone, cup, flower pot, lamp, tent, and vase [15, 48]. It’s unfair to use the following metrics to evaluate these symmetrical categories. To tackle this problem, we evaluate on total objects (TO) and the asymmetric objects (AO) by removing symmetrical objects in the following experiments, respectively.

4.2 Evaluation metrics

We evaluate the registration in terms of the isotropic rotation and translation error $Error(R) = \arccos \frac{tr(\hat{R}^{-1}R)-1}{2}$, $Error(t) = \|\hat{R}^{-1}t - \hat{t}\|_1$ proposed in RPMNet[15], where R, t and \hat{R}, \hat{t} represent the predicted and the ground truth transformation respectively, $tr(\cdot)$ means the trace of matrix. Moreover, we evaluate an-isotropic rotation and translation error $MAE(R), MAE(t)$ used in DCP [12] by calculating mean absolute error of Euler angle and translation vector. Both $Error(R)$ and $MAE(R)$ represent rotation error in degrees.

4.3 Comparison with other methods

We compare ROPNet against ICP and FGR [7, 9] and learning-based methods which include PCRNet, DCP-v2, IDAM-GNN, DeepGMR, and RPMNet [15, 12, 11, 14, 17]. We generate source and target point cloud X and Y in the style of twice sample by sampling 1024 points independently following RPMNet [15]. We randomly generate three Euler angles within $[0^\circ, 45^\circ]$ and translations within $[-0.5, 0.5]$ on each axis. For generating partial point cloud, we adopt the mode conducted in RPMNet [15] which projects all points to a random direction, and 30% points are removed for partial-to-partial registration. The following experiments are all performed in the partial-to-partial setting to evaluate on both AO and TO data of ModelNet40.

Unseen shapes We use 40 categories for training, then test both TO and AO data on the test set. The results in Table 1 indicate that our ROPNet outperforms the other methods with $Error(R)$ 0.7820, $Error(t)$ 0.0086 on AO, and $Error(R)$ 1.1567, $Error(t)$ 0.0108 on TO. It also shows that RPMNet outperforms DCP-v2, IDAM-GNN, DeepGMR, and ICP. Moreover, our ROPNet model always remains superior being still more than twice as fast as RPMNet illustrated in Figure 1.

Unseen categories We use the first 20 categories for training and the rest 20 categories for testing to validate the model generalization ability. As shown in Table 2, ICP and FGR obtain similar performances. IDAM-GNN and DeepGMR obtain higher error showing slightly weaker generalization ability. DCP-v2, RPMNet, ROPNet and PCRNet obtain similar or lower error showing great generalization ability. Overall, ROPNet outperforms all the compared methods in both AO and TO data.

Methods	AO				TO			
	$Error(R)$	$Error(t)$	$MAE(R)$	$MAE(t)$	$Error(R)$	$Error(t)$	$MAE(R)$	$MAE(t)$
ICP	23.7983	0.2512	12.0064	0.1180	25.4879	0.2504	12.8976	0.1183
FGR	15.6677	0.0934	9.6716	0.0443	15.3317	0.1036	9.4110	0.0491
PCRNet	21.0916	0.1900	10.5662	0.0929	21.5943	0.1915	10.7881	0.0933
DCP-v2	10.4008	0.1490	5.4455	0.0723	11.1543	0.1564	5.7080	0.0758
IDAM-GNN	15.9915	0.2109	8.4099	0.0991	17.3614	0.2153	8.9823	0.1022
DeepGMR	17.4120	0.1939	8.7646	0.0951	18.3608	0.1998	9.1425	0.0977
RPMNet	1.1273	0.0143	0.5987	0.0069	1.6781	0.0169	0.8749	0.0079
ROPNet	0.9285	0.0114	0.5029	0.0054	1.1637	0.0116	0.6190	0.0055

Table 2: Results on ModelNet40 unseen categories.

Methods	AO				TO			
	$Error(R)$	$Error(t)$	$MAE(R)$	$MAE(t)$	$Error(R)$	$Error(t)$	$MAE(R)$	$MAE(t)$
ICP	24.3766	0.2542	12.3258	0.1196	25.5219	0.2515	12.9118	0.1190
FGR	28.6681	0.1742	17.7317	0.0827	29.2813	0.1828	18.1986	0.1887
PCRNet	21.4136	0.1924	10.7220	0.0940	21.7476	0.1933	10.8870	0.0942
DCP-v2	10.8202	0.1508	5.6436	0.0734	11.5672	0.1578	5.9095	0.0765
IDAM-GNN	16.6100	0.2206	8.7257	0.1033	16.9805	0.2125	8.9366	0.1003
DeepGMR	17.8840	0.1972	8.9990	0.0967	18.8075	0.2027	9.3672	0.0992
RPMNet	1.2343	0.0157	0.6544	0.0075	1.7569	0.0177	0.9177	0.0084
ROPNet	1.1566	0.0137	0.6215	0.0066	1.4656	0.0145	0.7799	0.0070

Table 3: Results on ModelNet40 unseen categories with Gaussian noise.

Robustness evaluation We also evaluate the robustness of models in the presence of noise. The noise is sampled from $N(0, 0.01^2)$ and clipped to $[-0.5, 0.5]$. As shown in Table 3, FGR is sensitive to noise, and registration error grows sharply. On the contrary, other methods are robust to noise and obtain similar registration error. In addition, our method is still the best among all the methods with $Error(R)$ 1.1566, $Error(t)$ 0.0137 in AO data and $Error(R)$ 1.4656, $Error(t)$ 0.0145 in TO data. The registration visualization is illustrated in Figure 4.

4.4 Ablation study

Overlap prediction Table 4 (left) shows the precision and recall of the predicted overlapping points in X . The numbers in brackets indicate the threshold d defining in Equation 8. The CG module obtains 0.810 and 0.939 in precision with

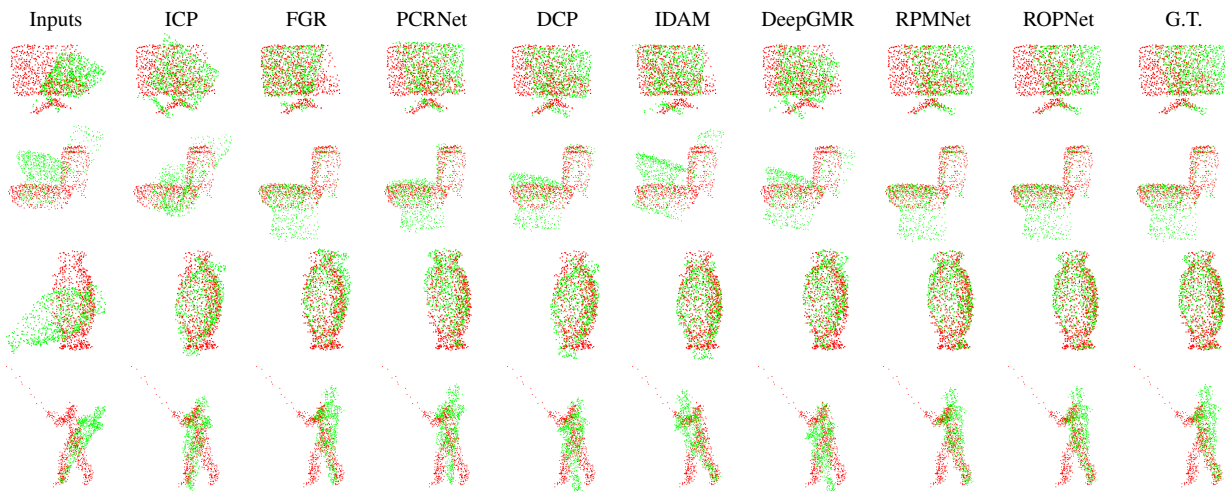


Figure 4: Registration visualization on ModelNet40 unseen categories with Gaussian noise. The source and target point cloud X, Y are marked in green and red respectively

	AO		TO		Correspondence	Global	Overlap	FMR	TO $Error(R)$	TO $Error(t)$
	OP (0.05, 0.07)	OR (0.05, 0.07)	OP (0.05, 0.07)	OR (0.05, 0.07)						
CG	0.810 / 0.939	0.836 / 0.822	0.806 / 0.936	0.838 / 0.824	✓	✓			5.9518	0.0843
CG + TFMR	0.913 / 0.987	0.382 / 0.347	0.908 / 0.984	0.382 / 0.348	✓	✓	✓		4.8219	0.0502
					✓	✓	✓		3.3361	0.0378
					✓	✓	✓	✓	1.9592	0.0189
					✓	✓	✓	✓	1.4656	0.0145

Table 4: Left: Overlap Precision (OP) and Recall (OR). Right: Ablation studies of different components for registration error. They are both on ModelNet40 unseen categories with Gaussian noise.

the threshold 0.05 and 0.07, respectively, demonstrating that most of the predicted overlapping points by CG module are positive or near positive overlapping points. With TFMR, ROPNet obtains better precision with 0.913 and 0.987 in the threshold of 0.05 and 0.07. The results reported in TO data showed the overlap prediction is also applicable to symmetric objects. Though OR drops with TFMR, some overlapping points removed in X are with poor descriptor introduced in subsection 3.2.

Registration error As shown in Table 4 (right), we regard the first row as the benchmark, which just learns point features and generates similarity matrix for registration. The second row and the third row demonstrate global context features for initialized alignment, and the overlap module can both reduce the rotation error and translation error. The overlap module boosts registration accuracy more. With a combination of coarse initialization and the overlap module, as shown in the fourth row, $Error(R)$, $Error(t)$ are reduced significantly to 1.9592, 0.0189. Furthermore, with FMR module, we gain the lowest error with $Error(R)$ 1.4656 and $Error(t)$ 0.0145.

5 Conclusion

We proposed ROPNet, a new method for partially overlapping point clouds registration. A context-guided (CG) module is introduced for initial alignment and overlapping points prediction. Based on the CG module, we included a TFMR module to extract point features based on all input points, obtain representative overlapping points, and transform partial-to-partial registration into partial-to-complete registration. Experiment results showed that ROPNet obtained the lowest error with robustness to noise and generalization ability to unseen shape categories while keeping efficiency. Future work should be considered to refine the design of the proposed network to operate on large-scale point clouds and expand its generalization to real-world scanned data.

References

- [1] Gérard Blais and Martin D. Levine. Registering multiview range data to create 3d computer objects. *IEEE Transactions on Pattern Analysis and Machine Intelligence*, 17(8):820–824, 1995.
- [2] Sungjoon Choi, Qian-Yi Zhou, and Vladlen Koltun. Robust reconstruction of indoor scenes. In *Proceedings of the IEEE Conference on Computer Vision and Pattern Recognition*, pages 5556–5565, 2015.
- [3] Michael Merickel. 3d reconstruction: the registration problem. *Computer vision, graphics, and image processing*, 42(2):206–219, 1988.
- [4] Weixin Lu, Yao Zhou, Guowei Wan, Shenhua Hou, and Shiyu Song. L3-net: Towards learning based lidar localization for autonomous driving. In *Proceedings of the IEEE/CVF Conference on Computer Vision and Pattern Recognition*, pages 6389–6398, 2019.
- [5] Guowei Wan, Xiaolong Yang, Renlan Cai, Hao Li, Yao Zhou, Hao Wang, and Shiyu Song. Robust and precise vehicle localization based on multi-sensor fusion in diverse city scenes. In *2018 IEEE International Conference on Robotics and Automation (ICRA)*, pages 4670–4677. IEEE, 2018.
- [6] Jay M Wong, Vincent Kee, Tiffany Le, Syler Wagner, Gian-Luca Mariottini, Abraham Schneider, Lei Hamilton, Rahul Chipalkatty, Mitchell Hebert, David MS Johnson, et al. Segicp: Integrated deep semantic segmentation and pose estimation. In *2017 IEEE/RSJ International Conference on Intelligent Robots and Systems (IROS)*, pages 5784–5789. IEEE, 2017.
- [7] P. J. Besl and N. D. McKay. A method for registration of 3-d shapes. *IEEE Transactions on Pattern Analysis and Machine Intelligence*, 14(2):239–256, 1992.
- [8] J. Yang, H. Li, D. Campbell, and Y. Jia. Go-icp: A globally optimal solution to 3d icp point-set registration. *IEEE Transactions on Pattern Analysis and Machine Intelligence*, 38(11):2241–2254, 2016.
- [9] Qian-Yi Zhou, Jaesik Park, and Vladlen Koltun. Fast global registration. In *European Conference on Computer Vision*, pages 766–782. Springer, 2016.

- [10] Yasuhiro Aoki, Hunter Goforth, Rangaprasad Arun Srivatsan, and Simon Lucey. Pointnetlk: Robust & efficient point cloud registration using pointnet. In *Proceedings of the IEEE/CVF Conference on Computer Vision and Pattern Recognition*, pages 7163–7172, 2019.
- [11] Vinit Sarode, Xueqian Li, Hunter Goforth, Yasuhiro Aoki, Rangaprasad Arun Srivatsan, Simon Lucey, and Howie Choset. Pcnnet: Point cloud registration network using pointnet encoding. *arXiv preprint arXiv:1908.07906*, 2019.
- [12] Yue Wang and Justin M Solomon. Deep closest point: Learning representations for point cloud registration. In *Proceedings of the IEEE/CVF International Conference on Computer Vision*, pages 3523–3532, 2019.
- [13] Yue Wang and Justin M Solomon. Prnet: Self-supervised learning for partial-to-partial registration. *arXiv preprint arXiv:1910.12240*, 2019.
- [14] Jiahao Li, Changhao Zhang, Ziyao Xu, Hangning Zhou, and Chi Zhang. Iterative distance-aware similarity matrix convolution with mutual-supervised point elimination for efficient point cloud registration. *arXiv preprint arXiv:1910.10328*, 2019.
- [15] Zi Jian Yew and Gim Hee Lee. Rpm-net: Robust point matching using learned features. In *Proceedings of the IEEE/CVF conference on computer vision and pattern recognition*, pages 11824–11833, 2020.
- [16] Shengyu Huang, Zan Gojcic, Mikhail Usvyatsov, Andreas Wieser, and Konrad Schindler. Predator: Registration of 3d point clouds with low overlap, 2021.
- [17] Wentao Yuan, Benjamin Eckart, Kihwan Kim, Varun Jampani, Dieter Fox, and Jan Kautz. Deepgmr: Learning latent gaussian mixture models for registration. In *European Conference on Computer Vision*, pages 733–750. Springer, 2020.
- [18] Kexue Fu, Shaolei Liu, Xiaoyuan Luo, and Manning Wang. Robust point cloud registration framework based on deep graph matching. In *Proceedings of the IEEE/CVF Conference on Computer Vision and Pattern Recognition*, pages 8893–8902, 2021.
- [19] Eric Jang, Shixiang Gu, and Ben Poole. Categorical reparameterization with gumbel-softmax. *arXiv preprint arXiv:1611.01144*, 2016.
- [20] Richard Sinkhorn. A relationship between arbitrary positive matrices and doubly stochastic matrices. *The annals of mathematical statistics*, 35(2):876–879, 1964.
- [21] Yang Chen and Gérard Medioni. Object modelling by registration of multiple range images. *Image and vision computing*, 10(3):145–155, 1992.
- [22] Szymon Rusinkiewicz and Marc Levoy. Efficient variants of the icp algorithm. In *Proceedings third international conference on 3-D digital imaging and modeling*, pages 145–152. IEEE, 2001.
- [23] Rahul Raguram, Jan-Michael Frahm, and Marc Pollefeys. A comparative analysis of ransac techniques leading to adaptive real-time random sample consensus. In *European Conference on Computer Vision*, pages 500–513. Springer, 2008.
- [24] Radu Bogdan Rusu, Nico Blodow, and Michael Beetz. Fast point feature histograms (fpfh) for 3d registration. In *2009 IEEE international conference on robotics and automation*, pages 3212–3217. IEEE, 2009.
- [25] Charles R Qi, Hao Su, Kaichun Mo, and Leonidas J Guibas. Pointnet: Deep learning on point sets for 3d classification and segmentation. In *Proceedings of the IEEE conference on computer vision and pattern recognition*, pages 652–660, 2017.
- [26] Bruce D. Lucas and Takeo Kanade. An iterative image registration technique with an application to stereo vision. In *IJCAI’81 Proceedings of the 7th international joint conference on Artificial intelligence - Volume 2*, pages 674–679, 1981.
- [27] Christopher Choy, Jaesik Park, and Vladlen Koltun. Fully convolutional geometric features. In *Proceedings of the IEEE/CVF International Conference on Computer Vision*, pages 8958–8966, 2019.
- [28] Olaf Ronneberger, Philipp Fischer, and Thomas Brox. U-net: Convolutional networks for biomedical image segmentation. In *International Conference on Medical image computing and computer-assisted intervention*, pages 234–241. Springer, 2015.
- [29] Xuyang Bai, Zixin Luo, Lei Zhou, Hongbo Fu, Long Quan, and Chiew-Lan Tai. D3feat: Joint learning of dense detection and description of 3d local features. In *Proceedings of the IEEE/CVF Conference on Computer Vision and Pattern Recognition*, pages 6359–6367, 2020.
- [30] Hugues Thomas, Charles R Qi, Jean-Emmanuel Deschaud, Beatriz Marcotegui, François Goulette, and Leonidas J Guibas. Kpconv: Flexible and deformable convolution for point clouds. In *Proceedings of the IEEE/CVF International Conference on Computer Vision*, pages 6411–6420, 2019.

- [31] Sheng Ao, Qingyong Hu, Bo Yang, Andrew Markham, and Yulan Guo. Spinnet: Learning a general surface descriptor for 3d point cloud registration, 2021.
- [32] Bertram Drost, Markus Ulrich, Nassir Navab, and Slobodan Ilic. Model globally, match locally: Efficient and robust 3d object recognition. In *2010 IEEE computer society conference on computer vision and pattern recognition*, pages 998–1005. Ieee, 2010.
- [33] Meng-Hao Guo, Jun-Xiong Cai, Zheng-Ning Liu, Tai-Jiang Mu, Ralph R Martin, and Shi-Min Hu. Pct: Point cloud transformer. *arXiv preprint arXiv:2012.09688*, 2020.
- [34] Hengshuang Zhao, Li Jiang, Jiaya Jia, Philip Torr, and Vladlen Koltun. Point transformer. *arXiv preprint arXiv:2012.09164*, 2020.
- [35] Nico Engel, Vasileios Belagiannis, and Klaus Dietmayer. Point transformer. *arXiv preprint arXiv:2011.00931*, 2020.
- [36] Charles R Qi, Li Yi, Hao Su, and Leonidas J Guibas. Pointnet++: Deep hierarchical feature learning on point sets in a metric space. *arXiv preprint arXiv:1706.02413*, 2017.
- [37] Yue Wang, Yongbin Sun, Ziwei Liu, Sanjay E Sarma, Michael M Bronstein, and Justin M Solomon. Dynamic graph cnn for learning on point clouds. *Acm Transactions On Graphics (tog)*, 38(5):1–12, 2019.
- [38] Yongcheng Liu, Bin Fan, Shiming Xiang, and Chunhong Pan. Relation-shape convolutional neural network for point cloud analysis. In *Proceedings of the IEEE/CVF Conference on Computer Vision and Pattern Recognition*, pages 8895–8904, 2019.
- [39] Yangyan Li, Rui Bu, Mingchao Sun, Wei Wu, Xinhan Di, and Baoquan Chen. Pointcnn: Convolution on χ -transformed points. In *Proceedings of the 32nd International Conference on Neural Information Processing Systems*, pages 828–838, 2018.
- [40] Hengshuang Zhao, Li Jiang, Chi-Wing Fu, and Jiaya Jia. Pointweb: Enhancing local neighborhood features for point cloud processing. In *Proceedings of the IEEE/CVF Conference on Computer Vision and Pattern Recognition*, pages 5565–5573, 2019.
- [41] Adam Paszke, Sam Gross, Soumith Chintala, Gregory Chanan, Edward Yang, Zachary DeVito, Zeming Lin, Alban Desmaison, Luca Antiga, and Adam Lerer. Automatic differentiation in pytorch. *31st Conference on Neural Information (NIPS 2017)*, 2017.
- [42] Adam Paszke, Sam Gross, Francisco Massa, Adam Lerer, James Bradbury, Gregory Chanan, Trevor Killeen, Zeming Lin, Natalia Gimelshein, Luca Antiga, et al. Pytorch: An imperative style, high-performance deep learning library. *arXiv preprint arXiv:1912.01703*, 2019.
- [43] Yuxin Wu and Kaiming He. Group normalization. In *Proceedings of the European conference on computer vision (ECCV)*, pages 3–19, 2018.
- [44] Diederik P Kingma and Jimmy Ba. Adam: A method for stochastic optimization. *arXiv preprint arXiv:1412.6980*, 2014.
- [45] Ilya Loshchilov and Frank Hutter. Sgdr: Stochastic gradient descent with warm restarts. *arXiv preprint arXiv:1608.03983*, 2016.
- [46] Zhirong Wu, Shuran Song, Aditya Khosla, Fisher Yu, Linguang Zhang, Xiaoou Tang, and Jianxiong Xiao. 3d shapenets: A deep representation for volumetric shapes. In *Proceedings of the IEEE conference on computer vision and pattern recognition*, pages 1912–1920, 2015.
- [47] Huanshu Wei, Zhijian Qiao, Zhe Liu, Chuanzhe Suo, Peng Yin, Yueling Shen, Haoang Li, and Hesheng Wang. End-to-end 3d point cloud learning for registration task using virtual correspondences. In *2020 IEEE/RSJ International Conference on Intelligent Robots and Systems (IROS)*, pages 2678–2683. IEEE, 2020.
- [48] Hao Xu, Shuaicheng Liu, Guangfu Wang, Guanghui Liu, and Bing Zeng. Omnet: Learning overlapping mask for partial-to-partial point cloud registration. *arXiv preprint arXiv:2103.00937*, 2021.

Appendix

A. Architecture

Context-guided encoder The encoder of the context-guided (CG) module is a PointNet without T-Net for transformations as shown in Figure 5 (left-top). It contains 5 Conv1d (64, 64, 64, 128, 512) and ReLU layers without normalization operations. It takes the point cloud X as input and outputs a 512-dimensional feature F_X for each point.

Initialization decoder The initial alignment decoder is a MLP that contains 4 FC (512, 512, 256, 7) and ReLU layers without normalization operations. It takes the fused global features $[F_X^g; F_Y^g]$ as input and outputs a 7-dimensional vector v representing the rotation and translation transformation

Overlap decoder The overlap decoder is a PointNet without T-Net for transformations as shown in Figure 5 (left-bottom). It contains 4 Conv1d (512, 512, 256, 2) and ReLU(except the last layer) layers without normalization operations. It takes the features output from the Information Interactive module and outputs an overlap score for each point.

Point cloud Transformer As shown in Figure 5 (right-bottom), the point cloud Transformer contains four attention blocks and concatenates outputs from each attention block as the final output features. As shown in Figure 5 (right-top), attention block is a offset attention which calculates the difference between the self-attention features and the input features. Each attention block outputs a 192-dimensional feature. Thus the output of the point cloud Transformer is 768-dimensional features. We use GN instead of BN in point cloud Transformer.

Loss function The total loss is the weighted summation of the three losses:

$$L_{total} = \alpha \cdot L_{fin} + \beta \cdot L_{ol} + \lambda \cdot L_{init}, \quad (9)$$

where α , β and γ are set to 1, 0.1 and 1, respectively.

B. Implementation Details

The number of reserved points (top- N_1) is 448 after removal operation based on overlap score. Top-*prob* is set to 0.6 and 0.4 for training and test, respectively. We set top-*k* to 3 and 1 for training and test, respectively. The overlap threshold d is set to 0.05. We train ROPNet in a non-iterative manner. However, we run 2 iterations for the TFMR module during test. For the ModelNet40 dataset, we train for 600 epochs, using Adam with an initial learning rate of 0.0001. The learning rate changes using a cosine annealing schedule with the first restart set to 40 iterations and an increasing factor of 2. We use batch size 8 in experiments. Data augmentation includes horizontal flip and adding Gaussian noise with $\sigma = 0.5$

C. Experiments

C.1 Benchmarks implementation details

We compare our method with traditional and learning-based methods, including ICP, FGR, PCRNet, DCP, IDAM, DeepGMR, and RPMNet. For a fair comparison, we evaluate them on the same test set (the same input point clouds and transformation matrix) and retrain them with the same generation strategy for point cloud pairs, randomly. ICP and FGR are implemented using the Open3D library. PCRNet and DeepGMR are designed for complete-to-complete registration. The proposed loss is invalid for partial-to-partial registration, so we modified the loss as conducted in RPMNet for effective training. It is also noted that the hand-crafted RRI features are not essential for DeepGMR, and we found that the training is not converging with RRI features as input, so we remove RRI features in both the training and testing stage. For DCP, we adopt DCP-v2 with an attention model and SVD. For IDAM, we train with both GNN-based features and PPFH-based features and find that they both overfit the training set, so we reported the results of IDAM-GNN model, which are better in performance. PRNet may be the first learning-based model to solve partial-to-partial registration. However, the code released by the authors is prone to collapse when training, so we don't use it for comparison in this work.

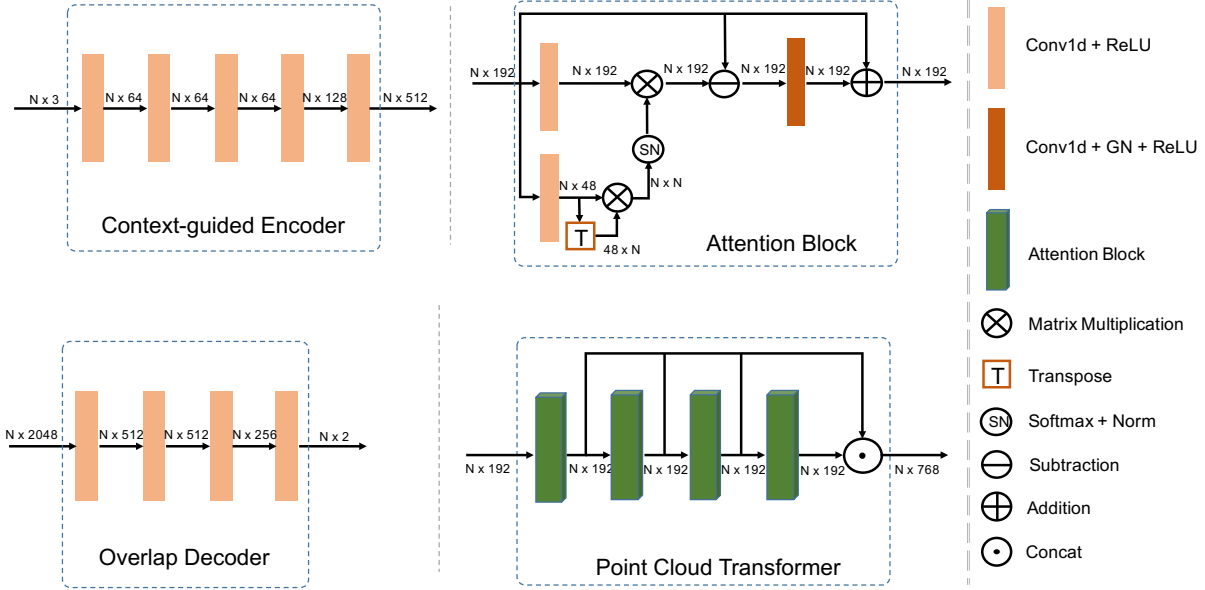


Figure 5: Left-top: Architecture of encoder of context-guided module. Left-bottom: Architecture of overlap decoder. Right-top: Attention block for point cloud Transformer. Right-bottom: Architecture of point cloud Transformer.

C.2 Ablation study

The following experiments in this subsection are all conducted on the ModelNet40 unseen categories with Gaussian noise.

Number of iterations We evaluated $Error(R)$ and $Error(t)$ based on different iterations. The results are shown in Figure 6. As the number of iterations increases, the error decreases. The error drops sharply in the second iteration. Considering the running time, we only iterate two times in our ROPNet.

Top- N_1 Based on overlap score, we keep top- N_1 points in source point cloud X for registration. As shown in Figure 7, we evaluated $Error(R)$ and $Error(t)$ for different $N_1 \in \{717, 560, 448, 336, 224\}$. We obtained sub-optimal registration results based on all points (717) for registration, because some points are non-overlapping points. We obtained the lowest error based on 448 points for registration.

Top- $prob$ Based on feature matching, we keep top- $prob$ points for registration whose features are descriptive. We evaluated $Error(R)$ and $Error(t)$ based on different top- $prob$ with values: 0.2, 0.4, 0.6, 0.8 and 1. As shown in Figure 8, all points (top- $prob = 1$) for registration is sub-optimal due to selected points are not representative. We obtained the best performance based on top- $prob = 0.4$.

Top- M_1 Based on overlap score, we keep top- M_1 points in target point cloud Y for registration. As shown in Figure 9, we evaluate the $Error(R)$ and $Error(t)$ for different values $M_1 \in \{717, 560, 448\}$. We obtained the lowest error based on all points (717) for registration, demonstrating that some overlapping points, mistakenly removed from the target point cloud, affect the registration.

C.3 Additional experiments

Representative overlapping points Here, we visualize the representative overlapping points on ModelNet40 unseen categories with Gaussian noise. As shown in Figure 10, the CG module predicts the overlapping (or nearly overlapping) points. The TFMR module removes the non-representative points (including some non-overlapping points shown in the purple rectangles) based on feature matching.

Unseen shapes Figure 11 shows 14-classes of the ModelNet40 unseen shapes. We select the 10-classes in the first 20 classes in stride two and beginning 0. Also, we select four classes in the last 20 classes. The classes include airplane, bed, bookshelf, bowl, chair, cup, desk, dresser, glass box, keyboard, laptop, piano, sofa, and toilet.

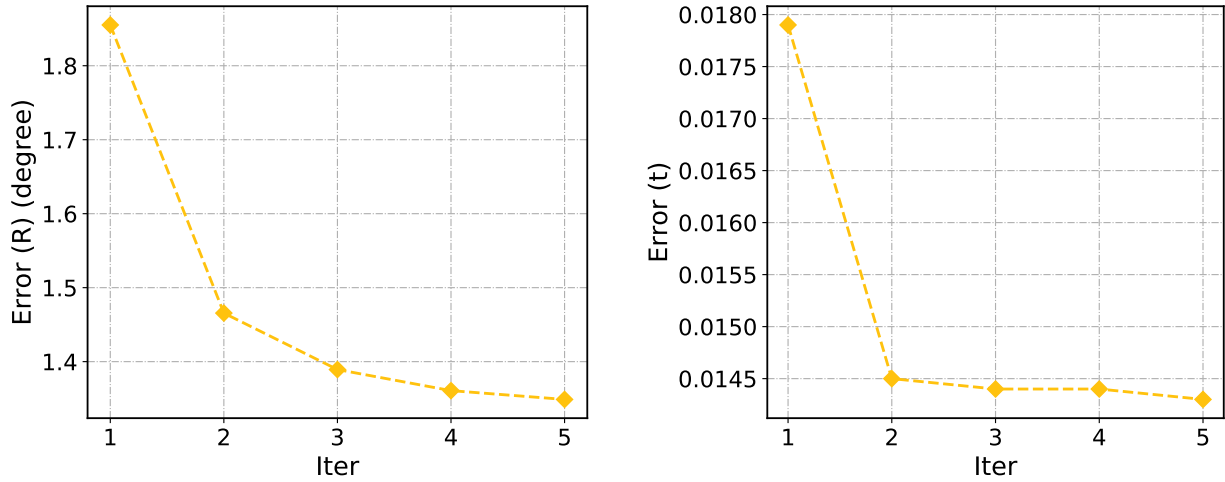


Figure 6: Left: $Error(R)$ with different iterations. Right: $Error(t)$ with different iterations.

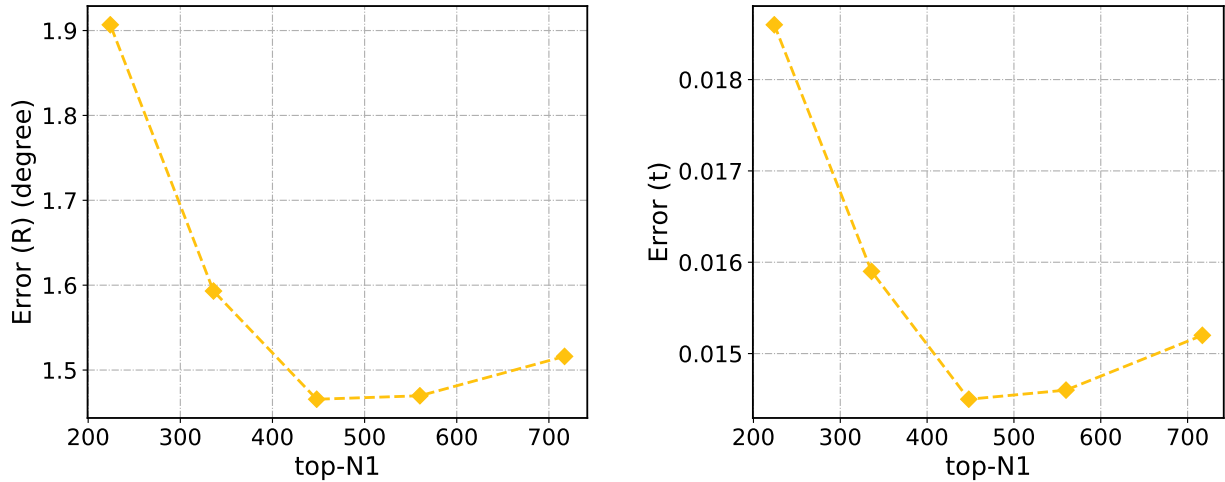


Figure 7: Left: $Error(R)$ with different N_1 . Right: $Error(t)$ with different N_1 .

Unseen categories Figure 12 shows 10-classes of the ModelNet40 unseen categories. We select the 10-classes in the last 20 classes in stride two and beginning 21. The classes include mantel, nightstand, piano, radio, sink, stairs, table, toilet, vase, and xbox.

Unseen categories with Gaussian noise Figure 13 shows 10-classes of the ModelNet40 unseen categories with Gaussian noise. We select the 10-classes in the last 20 classes in stride two and beginning 20. The classes include laptop, monitor, person, plant, range hood, sofa, stool, tent, tv stand, and wardrobe.

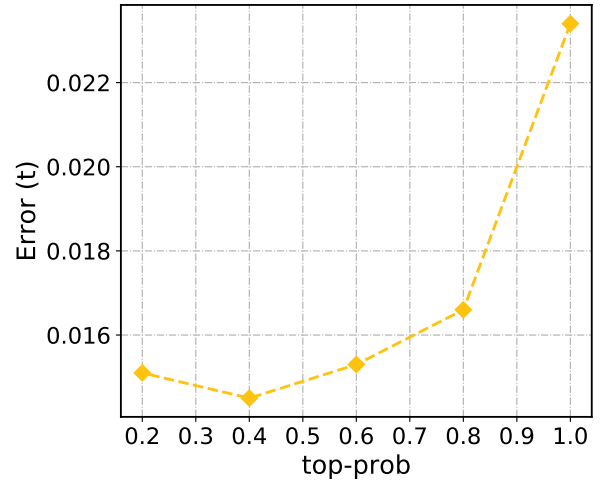
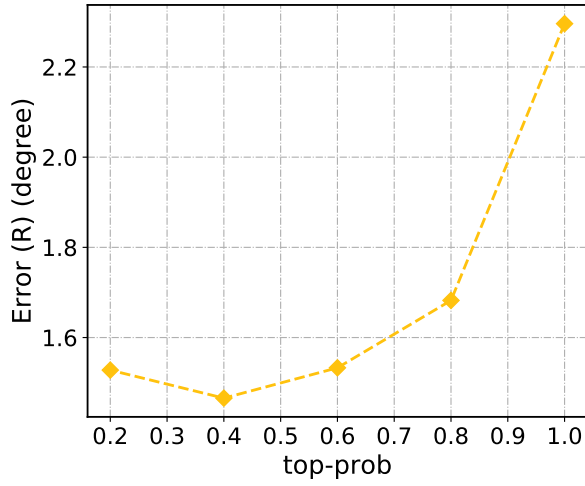


Figure 8: Left: $Error(R)$ with different $top-prob$. Right: $Error(t)$ with different $top-prob$.

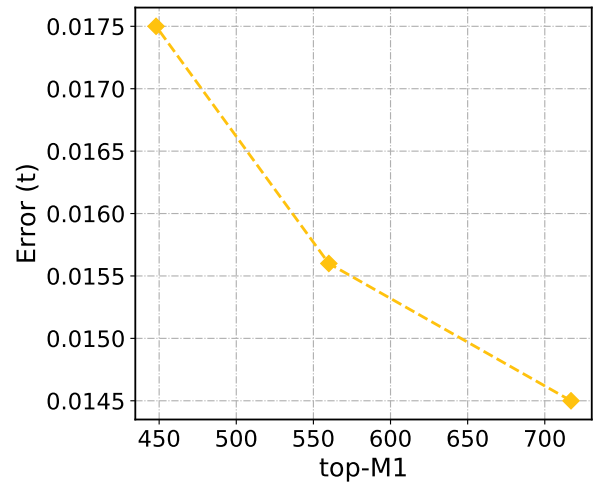
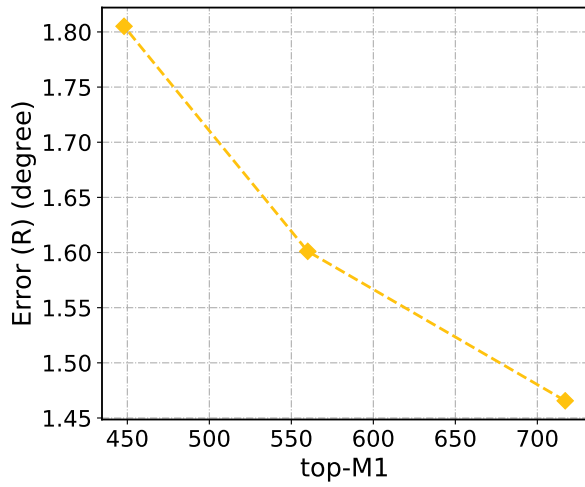


Figure 9: Left: $Error(R)$ with different M_1 . Right: $Error(t)$ with different M_1 .

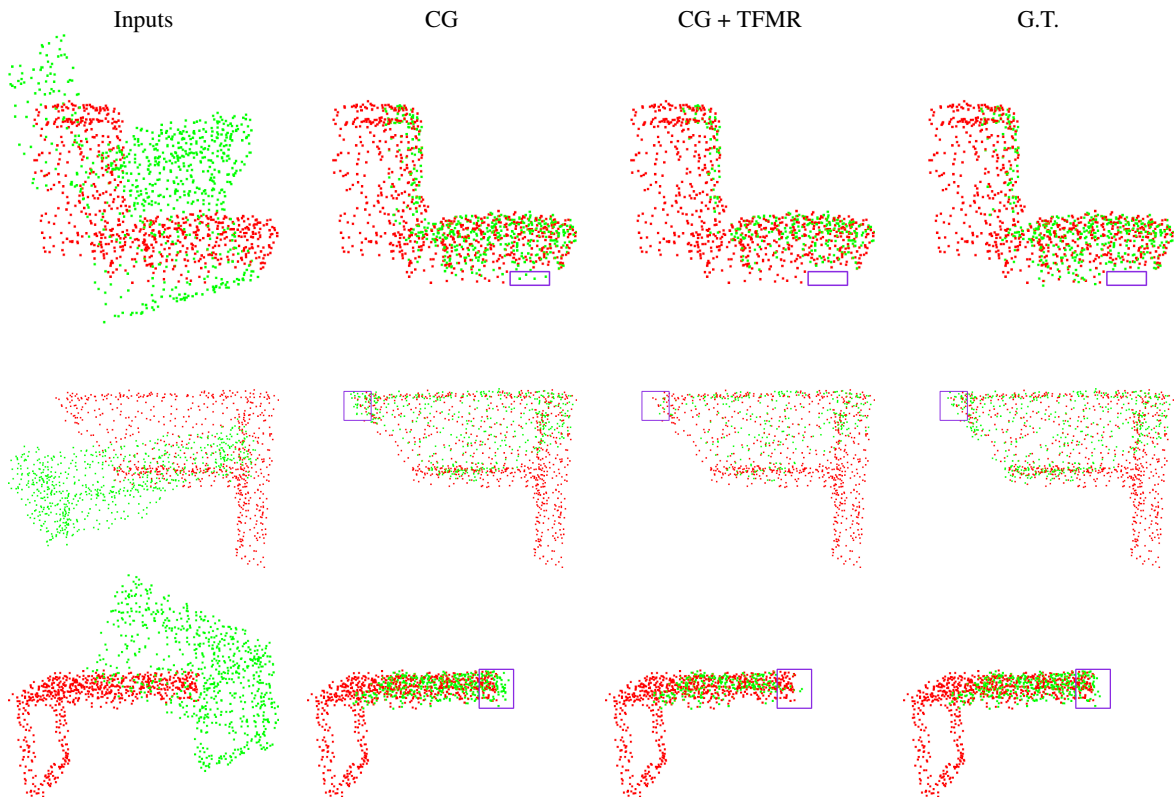


Figure 10: Predicted representative overlapping points on ModelNet40 unseen categories with Gaussian noise. The source and target point cloud X, Y are colored in green and red, respectively. The second column shows the predicted overlapping points in X by the CG module. As shown in the third column, TFMR further removes non-representative points based on feature matching, including some non-overlapping points depicted in purple rectangles. The last column shows the ground truth overlapping points in X .



Figure 11: Registration results on ModelNet40 unseen shapes. The source and target point clouds X, Y are colored in green and red, respectively

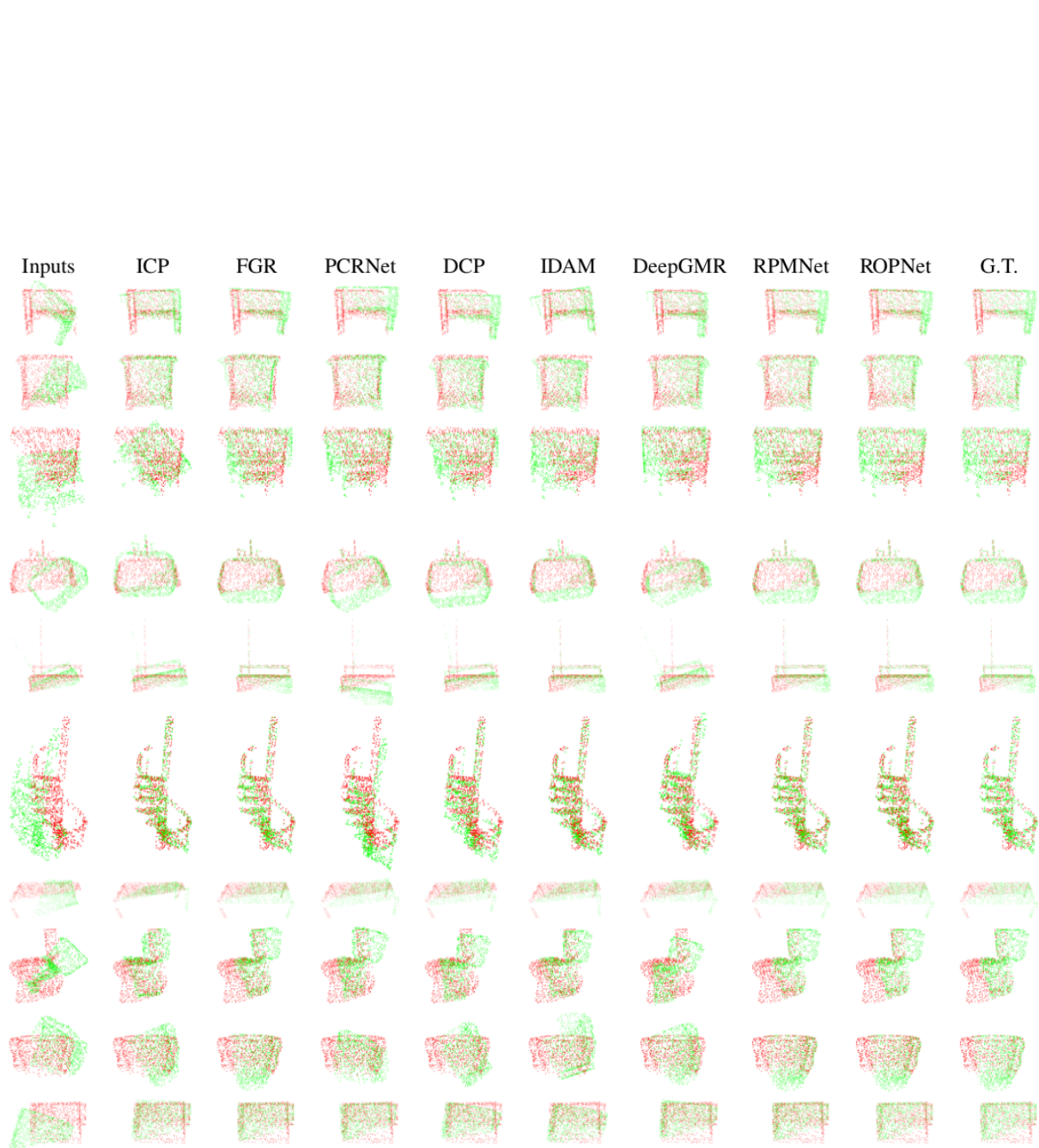


Figure 12: Registration results on ModelNet40 unseen categories. The source and target point clouds X, Y are colored in green and red, respectively

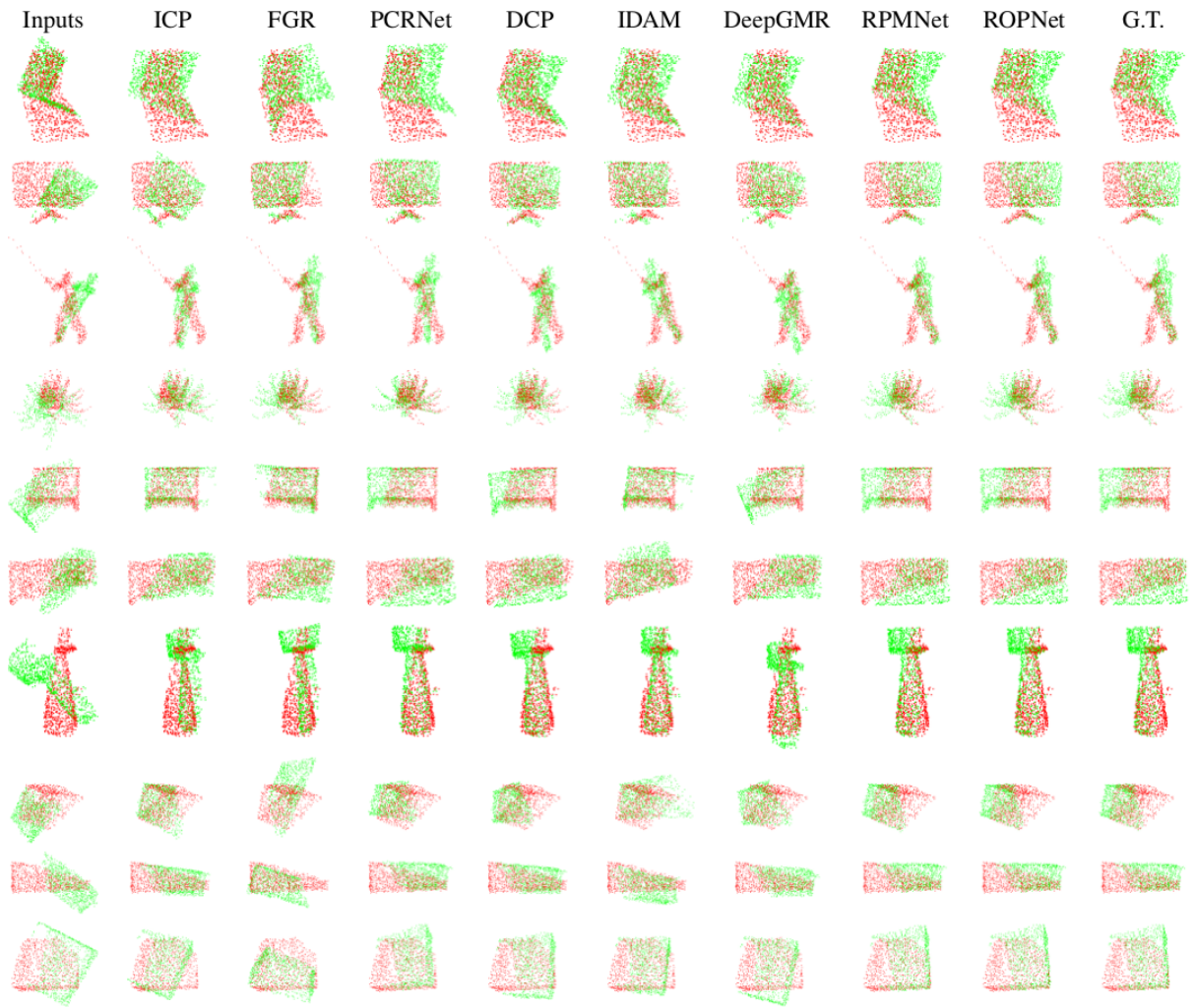


Figure 13: Registration results on ModelNet40 unseen categories with Gaussian noise. The source and target point clouds X, Y are colored in green and red, respectively